Elsevier Editorial System(tm) for
Microporous & Mesoporous Materials
Manuscript Draft

Manuscript Number: MICMAT-D-19-02173

Title: Re-examining the interpretation of CO adsorbed on Lewis acid sites of alkali metal-exchanged MOR zeolite

Article Type: Full length article

Keywords: CO; zeolites; Lewis acid sites; ab initio calculations; isosteric heats; IR spectra

Corresponding Author: Dr. Miroslav Rubes,

Corresponding Author's Institution:

First Author: Roman Bulánek

Order of Authors: Roman Bulánek; Eva Koudelková; Michal Trachta; Ota Bludský; Miroslav Rubes

Abstract: The interaction of CO with alkali metal-exchanged mordenite has been investigated by means of IR spectroscopy and calorimetry along with theoretical calculations based on DFT corrected to coupled-cluster accuracy (DFT/CC). It has been convincingly shown that Li+ is at least partially exchanged into the constricted part of the MOR structure as manifested by the low-frequency band at 2181 cm-1 and the isosteric heat of 44 kJ/mol. In the case of Na-MOR samples, significant changes have been observed in the stabilities of high- (2177 cm-1) and low-frequency (2165 cm-1) bands upon CO desorption, with the change of the Si/Al ratio from 40 to 9. Based on the kinetic measurements, it can be concluded that a crucial role in the MOR material is played by diffusion limitations, which are significantly influenced by the Si/Al ratio and the size of the cations. Similar effects also result in the increased stability of the 2138 cm-1 band of Na/K-MOR samples with higher Al content, where the "gate" effect is observed upon N2 adsorption. The dual cationic sites are directly observed only for the K-MOR sample via the weak band around 2150 cm-1. The formation of dual cationic sites cannot be completely ruled out in the case of Na-MOR, but their presence is most likely hidden in the low-frequency band.

Cover Letter

ÚOCHB AV ČR
IOCB PRAGUE
Ústav organické chemie a biochemie
Akademie věd České republiky, v. v. i.
Institute of Organic Chemistry and Biochemistry
of the Czech Academy of Sciences

Editor
W. Schmidt

06.11.2019

Dear Prof. Schmidt,

we would like to submit an article entitled “Re-examining the interpretation of CO adsorbed on Lewis acid sites of alkali metal-exchanged MOR zeolite” by R. Bulanek, E. Koudelkova, M. Trachta, O. Bludsky and M. Rubes. There has been a tremendous interest in alkali exchanged **MOR** materials, however, some of the aspects of its behavior were not explain satisfactorily. We think that a combination of our experimental measurements and theoretical calculations explains quite well some of the puzzling features such as the presence of dual cationic sites and FT-IR band assigment. We think that Microporous and Mesoporous materials is a right platform to present our results.

Best regards,

Miroslav Rubes

Flemingovo nám. 2
166 10 Praha 6
Czech Republic

+420 220 183 333
uochb@uochb.cas.cz
www.uochb.cz

IČ: 61388963
DIČ: CZ61388963

***Reviewer Suggestions**

Prof. Silvia Bordiga, University of Turin, silvia.bordiga@unito.it
Prof. Konstantin Ivanov Hadjiivanov: Bulgarian Academy of Science, kih@svr.igic.bas.bg
Prof. Ben Slater: UCL, b.slater@ucl.ac.uk

Highlights

- The CO barrier to pass through channel constriction is about 40 $kJ.mol^{-1}$
- Li^{+} cation at least partially exchanges into constricted part of the **MOR** channel
- Kinetic stability of CO IR bands depends on Si/Al ratio
- The CO steric hindrance by larger cations (at low Si/Al ratio) most likely causing the increased stability of 2138 cm^{-1} band
- Dual cationic sites can be directly observed only for K-**MOR** material

***Graphical Abstract**

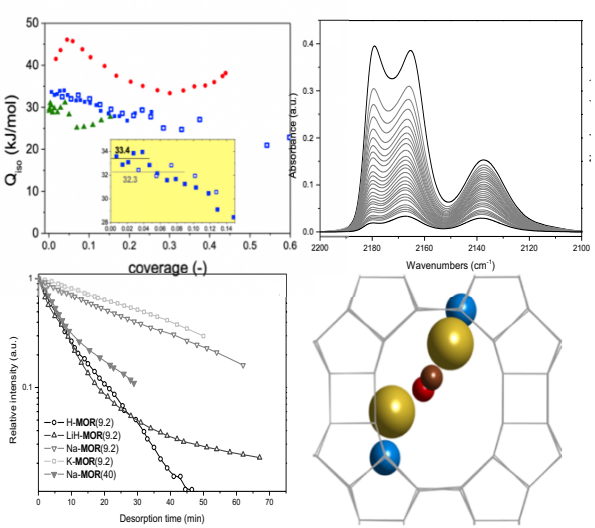

Re-examining the interpretation of CO adsorbed on Lewis acid sites of alkali metal-exchanged MOR zeolite

Roman Bulánek[1], *Eva Koudelková*[1], *Michal Trachta*[2], *Ota Bludský*[2], *Miroslav Rubeš*[2]

[1] Department of Physical Chemistry, Faculty of Chemical Technology, University of Pardubice, Studentská 573, 532 10 Pardubice, Czech Republic

[2] Institute of Organic Chemistry and Biochemistry, Academy of Sciences of the Czech Republic, Flemingovo nám. 2, 162 10 Prague, Czech Republic

E-mail: miroslav.rubes@uochb.cas.cz

KEYWORDS

CO, zeolites, Lewis acid sites, ab initio calculations, isosteric heats, IR spectra

ABSTRACT

The interaction of CO with alkali metal-exchanged mordenite has been investigated by means of IR spectroscopy and calorimetry along with theoretical calculations based on DFT corrected to coupled-cluster accuracy (DFT/CC). It has been convincingly shown that Li^+ is at least partially exchanged into the constricted part of the **MOR** structure as manifested by the low-frequency band at 2181 cm^{-1} and the isosteric heat of 44 kJ/mol. In the case of Na-**MOR** samples, significant changes have been observed in the stabilities of high- (2177 cm^{-1}) and low-frequency (2165 cm^{-1}) bands upon CO desorption, with the change of the Si/Al ratio from 40 to 9. Based on the kinetic measurements, it can be concluded that a crucial role in the **MOR** material is played by diffusion limitations, which are significantly influenced by the Si/Al ratio and the size of the cations. Similar effects also result in the increased stability of the 2138 cm^{-1} band of Na/K-**MOR** samples with higher Al content, where the "gate" effect is observed upon N_2 adsorption. The dual cationic sites are directly observed only for the K-**MOR** sample via the weak band around 2150 cm^{-1}. The formation of dual cationic sites cannot be completely ruled out in the case of Na-**MOR**, but their presence is most likely hidden in the low-frequency band.

1 Introduction

Zeolite mordenite (**MOR**) is one of the most used zeolites in industrial catalytic applications; its properties make it important for the future of sustainable chemistry.[1,2] The main channel is formed by 12-membered rings interconnected via constricted side channels, which are often called side pockets due to the diffusion limitations of most adsorbates through deformed 8-membered rings (Figure 1). For most adsorbates, **MOR** consequently acts as a 1-dimensional system, which makes the material a convenient catalyst for bulkier molecules such as C5/C6 hydrocarbons in processes such as gas purification, separation and/or drying.

The proton and alkali metal-exchanged forms of **MOR** have been studied numerous times both experimentally and theoretically to gain deeper insight into the character of catalytically active Brønsted/Lewis acid sites (BAS/LASs).[3–25] Although tremendous progress has been made, some characteristics of **MOR** active sites remain open. One of the most prominent ones is the presence of dual cationic sites (where the adsorbate interacts with two cations at the same time).[26,27] It has been shown that theirs presence can be investigated via carbon monoxide adsorption.[10,14,23,28–33] The CO is a very good IR probe due to its sensitivity to its environment; however, the CO bands observed in M-**MOR** (M= Li, Na or K) are slightly more difficult to interpret than in other conventionally used materials (e.g. ZSM-5). This complexity most likely arises from the presence of constricted 8-membered rings, where the cations are extremely well coordinated. The "standard" assignment of the three main CO bands is as follows: (i) the high-frequency (*hf*) band corresponds to CO interaction with cations in the main channel; (ii) the low-frequency (*lf*) band is assigned to CO interaction with cations at the channel constriction; and (iii) a band around 2138 cm^{-1}, which is common to most zeolites and is assigned to a non-specific CO interaction with zeolite channel walls. The dual cationic sites have already been discussed in the work of Salla et al.[21] for the Na-**MOR** material, where the increased stability of 2138 cm^{-1} was regarded as an indication of their presence. Nevertheless, this decrease in CO frequency with respect to the *hf* band of 2177 cm^{-1} seems to be too large to be interpreted as a dual cationic site.[26] Moreover, the sodium forms of most zeolites are less prone to form dual cationic sites than the potassium forms because of the possible incorporation of sodium cations into 6-membered rings of zeolitic structures.[34] In order to resolve the issue fully, we have compared Li-, Na- and K-**MOR** zeolites via measurements of CO IR bands along with a theoretical DFT/CC[35] model. Furthermore, it seems that the lithium cation cannot be exchanged fully into **MOR** and some protons always

remain in the structure.[10,16] Bordiga et al.[10] have concluded based on FT-IR of Li/Na/K-**MOR** that Li^+ is preferentially exchanged into the main channel and that cation positions at channel constrictions are those that are not exchanged. Their argument was supported by the large hydration sphere of Li^+ with respect to Na^+/K^+, which in general makes the lithium exchange slower than for other cations. Their conclusions were further supported by other works where the partial exchange of H-**MOR** into sodium forms was carried out.[16] On the other hand, when the frequencies of the remaining BAS sites are considered, a more complex picture might be in play.

Synthesized **MOR** materials usually have the Si/Al ratio between 5 and 11 (i.e. 4–8 Al atoms in the **MOR** unit cell). There is general agreement that Al is preferentially incorporated into **MOR** 4-membered rings (i.e. T_3 and T_4 positions).[36] This conclusion is only partially supported by computational studies, but the complexity of the synthetic process precludes theory from solving this issue in a definite manner.[3,17,24,37] Furthermore, the "real" Al distribution in low- to medium-Si/Al ratios in **MOR** is hard to predict computationally, because the stability of various cationic positions is highly dependent on model size due to the long-range character of the electrostatic interactions.[27,30,34] This work presents a combined theoretical and experimental study focusing on CO adsorption in alkali metal-exchanged **MOR** materials. A comparison can be readily made for various Si/Al ratios. The **MOR** sample with high silica content (Si/Al=40) can be, to a reasonable degree, compared with theoretical calculations for isolated adsorptions sites. The second **MOR** sample had higher Al content (Si/Al=9), which made the presence of dual cationic sites more likely. These sites can be at least qualitatively modeled via two-Al models, where two cations are arranged in a preferential way to form dual cationic sites in the **MOR** structure.

2 Methods

2.1 Materials and Experimental Details

The parent NH_4-**MOR**(9) zeolite was purchased from the TOSOH company, whereas NH_4-**MOR**(40) was synthesized based on the procedure described in Ref.[38] The ammonium forms of zeolites were converted to protonic ones by heating from room temperature to 723 K with the heating rate of 1 K min^{-1} in the flow of dry nitrogen and kept at this temperature for 1 h. Alkali metal-exchanged samples were prepared by the conventional ion-exchange procedure repeated five times, carried out in aqueous solution of appropriate nitrates (0.5 M) at 313 K for 1 day. Similarly to a previous study, the Li^+ could not be exchanged fully from the parent H-**MOR** material (hereinafter denoted as LiH-**MOR**) although the time of exchange was significantly increased (up to one week). In order to study partially exchanged Na-**MOR**(9) samples, the starting H-**MOR**(9) sample was exchanged at 313K for 5 h in 0.01, 0.1 and 1 M solutions of $NaNO_3$. The final samples were carefully washed by re-distilled water and dried at 373K in air overnight. The samples are denoted as M-**MOR**(x), where M stands for the cation type (H, Li, Na or K) and (x) stands for the Si/Al ratio. Partially exchanged Na-**MOR** samples are labeled as Na(x)H-**MOR**(9), where x stands for the concentration of the $NaNO_3$ solution used for ion exchange. The details of the basic characteristics of the materials (X-ray diffraction (XRD), scanning electron microscopy (SEM) and N_2 adsorption isotherms) are reported in the Supporting Information in Table S1 and Figures S1 and S2.

Carbonyls formed upon the adsorption of CO on the samples investigated were studied by FT-IR spectroscopy. For this purpose, the samples were pressed into self-supporting wafers with a density of 10 mg cm^{-2} and placed into a home-made low-temperature IR cell for transmission measurement allowing *in situ* activation (outgassing) and controlled dosing of the adsorbate to the cell. The samples were activated by slow heating at the rate of 1 K min^{-1} in a dynamic vacuum up to a temperature of 723 K, at which the sample was left for 10 h. Subsequently, the samples were freely cooled down to room temperature and then to the temperature of liquid nitrogen. Infrared spectra were recorded with an optical resolution of 2 cm^{-1} by the accumulation of 64 scans on a Nicolet 6700 FTIR spectrometer equipped with an MCT/A cryodetector. The carbon monoxide (99.997 purity) used in the study was purified by a freeze–pump–thaw cycle. The adsorption of CO was performed by dosing gas up to the equilibrium pressure of 1.1 mbar and waiting for 1 h for the equilibrium to be reached. After

that, desorption of CO was started by dynamic evacuation by a turbomolecular pump and IR spectra were collected each minute.

The kinetics of carbonyl formation on Na-**MOR** samples were studied by the measurement of time-dependent IR spectra after the dosing of a fixed amount of CO (2 μmol) to the sample at the temperature of liquid nitrogen on a Nicolet iS50 FTIR spectrometer equipped with an MCT/D cryodetector. Infrared spectra were recorded each second by accumulation of 1 scan with an optical resolution of 2 cm^{-1} in Spectra Series Omnic software extension.

Adsorption heats of CO on the samples investigated were measured on an isothermal Tian-Calvet type microcalorimeter (BT 2.15) combined with a volumetric/manometric device equipped with three capacitance pressure gauges for pressures up to 10 Torr, 100 Torr and 1000 Torr (Pfeiffer Vacuum). Prior to the experiments, the samples were outgassed *ex situ* by slowly increasing temperature under dynamic vacuum up to 723 K and kept at this temperature for 10 h. The calorimetric cell with the outgassed sample was transferred under vacuum into the calorimeter, after which the system was thermally equilibrated for at least 6 h. The heats of adsorption were measured at 303K by a step-by-step introduction of a small amount of CO (99.997 purity) into the cell. After each dose, the system was equilibrated for 60 minutes. The heat of adsorption was calculated by numerical differentiation of integral adsorption heat (obtained by the integration of the peak of heat-flow in time) by the amount adsorbed obtained from the volumetric/manometric adsorption isotherm measured simultaneously with heat flow.

2.2 Computational Details

Periodic DFT calculations were performed with the PBE[39] functional for the **MOR** 1x1x2 cell (a=18.256 b=20.543 c=15.084 Å with $\alpha=\beta=\gamma=90°$) (Figure 1).[40] The plane-wave energy cutoff was set to 400 eV and the Γ-point sampling of the first Brillouin zone was found to be sufficient. The gradients were converged to 0.01 eV/Å and zero-point vibrational energy (ZPVE) was calculated via the finite-difference approach using four displacements (0.005 Å) along each Cartesian coordinate of CO. Periodic DFT calculations were performed with PAW[41] pseudopotentials using the VASP[42] program package. A posteriori correction to the missing non-local correlation of the PBE functional (i.e. dispersion) was done with the PBE/CC approach as defined in Ref.[28]

Figure 1 The super cell (2x2x1) of mordenite with indicated 12-membered main channel (red ball), side pockets (blue ball) and constrictions in the side channel (green ball). The red- and green-ball diameters of 6.45 Å and 2.95 Å correspond to the maximum diameter for the ball to be able to diffuse along the main and side channels, respectively. The diameter of the blue ball of about 4.85 Å corresponds to the maximum diameter of the ball that can be accommodated inside the side pockets.

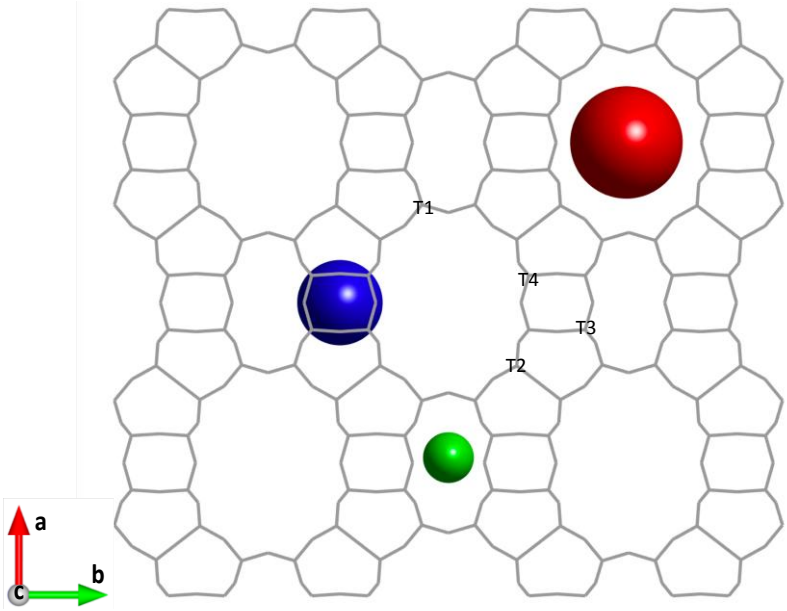

The models of the M-**MOR** (M= Li, Na and K) active sites were obtained by replacing silicon atom(s) with aluminum; the negative charge was compensated with the corresponding alkali metal cation forming Lewis acid centers. The **MOR** zeolite has four distinct T positions (denoted as T_x, where x=1–4) in which the aluminum can be exchanged. The **MOR** framework atoms are numbered according the IZA[40] notation. The adsorption-site notation is defined as follows: T – site, cationic position (M – main channel, I – intersection, and S – side pocket/channel), the parentheses with the *n*R value indicate the size of the zeolitic ring in which the cation resides. The CO position on each of the adsorption sites is indicated by a slash, where M/S denotes the main channel (M) and a side pocket/channel (S), respectively. For example, the T_2I(8R)/M adsorption site means that Al is in T_2, the compensating cation is at the channel intersection in the 8-membered ring, and CO is positioned in the main channel.

Vibrational CO frequencies were calculated by the *ω/r* correlation[43] as defined in Eq. (1):

$$\omega[cm^{-1}] = a\left[cm^{-1}\,\text{Å}^{-1}\right] * r_{X-X}^{DFT}[\text{Å}] + b[cm^{-1}] + \Delta v[cm^{-1}] \quad (eq\ 1),$$

where r_{X-X}^{DFT} is the CO distance obtained from PBE optimization; *a* and *b* parameters have been obtained from a fitting on series of model systems, where correlation between CCSD(T) vibrational frequency and r_{X-X}^{DFT} is established; and the $\Delta\nu$ is an additional correction term accounting for the anharmonicity of the CO vibration. Besides its computational benefits (Hessian does need to be calculated), the *ω/r* correlation has been shown to provide better accuracy than the DFT description of CO stretching frequency in zeolites.[26,29–31] The *ω/r* parameters for M-**MOR** (M=Li, Na, K) are summarized in Table S2.

The reference CCSD(T)[44] calculations at the complete basis set limit (CBS) have been performed to evaluate the PBE accuracy of CO interaction with the investigated cations in M-**MOR** materials (M= Li, Na and K). A more detailed description of the reference calculation is provided in the Supporting Information.

3 Results and Discussion

The stability of isolated (single) sites for Li/Na/K-**MOR** is summarized in Table S4, whereas the most stable structures are shown in Figures S3–S5. The obtained results can be summarized as follows: (i) at the T_1 position, only Li^+ prefers to be in the main channel at the small 6-membered ring, while Na^+/K^+ prefer to be inside the 8-membered ring of the side pocket, although in the case of Na^+ the energy difference between these two positions is rather small (3.2 kJ/mol); (ii) at the T_2 position, Li^+ prefers the small 5-membered ring in the main channel and Na^+/K^+ prefer the 8-membered ring at the intersection effectively blocking the access to the side pocket; (iii) at the T_3 position, all cations exchange into the constricted 8-membered ring, with Li^+ and K^+ being slightly better accessible from one of the side pockets; (iv) at the T_4 position, all cations preferentially exchange into the 8-membered ring at the channel intersection effectively blocking the accessibility of the side pockets.

The **MOR** material is usually considered a 1-dimensional system with side pockets because of the presence of channel constriction in the *b*-direction (Figure 1). However, the CO adsorbate is quite small and, on the time scale of the experimental measurements, it might be possible to pass through the channel constriction and form complexes at T_2 and T_4 intersection sites, where the CO is confined inside the side pocket. In order to avoid speculation, we have calculated a barrier of about 40 kJ/mol to push CO via the channel constriction using the dimer method.[45] Although this approach is only approximate, it is possible to conclude that the size of the barrier is not sufficient to prevent CO from passing through the channel constriction.

3.1 LiH-MOR

The FT-IR spectra of the LiH-**MOR** material are shown in Figure 2. There is a clear appearance of Li^+-CO species when the sample is evacuated. The evacuation needs to be performed to eliminate the interaction of CO with the remaining BAS sites, which is indicated by the disappearance of the bands around 2172 cm^{-1} and 3305 cm^{-1}, corresponding to C-O and O-H vibrations of residual BAS-CO, respectively.

Figure 2 The FT-IR spectra of CO interacting with LiH-**MOR**(9) at the temperature of liquid nitrogen: a sample in equilibrium with 1.1 mbar of CO (a) and upon dynamic evacuation at the same temperature for 40 min (b), 80 min (c), 150 min (d) and 190 min (e). Left bottom inset: the FT-IR spectrum of C-O vibrations on a sample after 150 min of evacuation represents stable Li-carbonyls and their deconvolution.

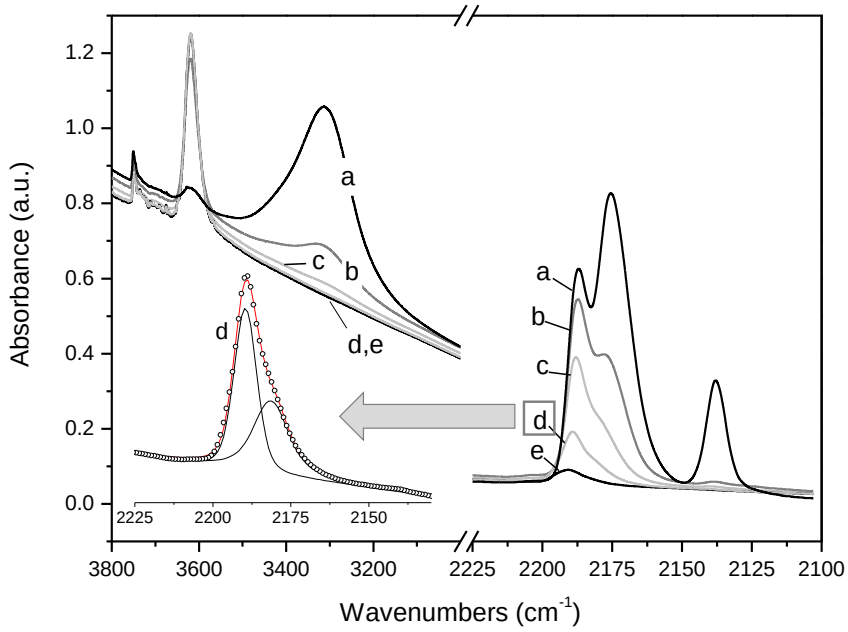

Table 1 The DFT/CC interaction energy and adsorption enthalpy (in kJ/mol) of CO\Li-**MOR** LASs along with *ω/r* CO frequencies (in cm^{-1}).

Ads. site[a]	E_{int}[b]	$-\Delta H_0$	ν_{CO}[c]	Band
T_1M(6R)/M	-39.8(-30.8)	36.9	2188	*hf*
T_1S(8R)/S	*-44.1(-22.1)*	*40.3*	*2175*	*lf*
T_2M(5R)/M	-41.0(-31.3)	37.9	2187	*hf*
T_3S(8R)/S	-47.8(-23.2)	43.6	2182	*lf*
T_4I(8R)/M	-43.3(-33.5)	40.0	2191	*hf*
T_4I(8R)/S	-41.6(-22.7)	38.3	2187	*hf*

[a] Less stable isolated sites are in italics (Table S4).

[b] PBE interaction energy is given in parentheses.

[c] CO gas-phase frequency is 2143 cm^{-1}.

There are two distinct CO bands corresponding to the Li^+-CO species: the *hf* band at 2189 cm^{-1} and the *lf* band at 2181 cm^{-1}. The theoretical calculation of the isolated CO\Li-**MOR** sites is summarized in Table 1. The *lf* band corresponds to Li^+-CO complexes with Al at the T_3 position (Figure 3), whereas the *hf* band corresponds to the remaining Al positions (i.e. T_1, T_2

and T_4). The band at 2175 cm^{-1} has not been observed in FT-IR spectra, most likely because of the lower stability of the $T_1S(8R)$ Li^+ site and the preferential incorporation of Al into **MOR** 4-membered rings, resulting in a higher population of T_3 and T_4 sites. High CO loading leads to the appearance of the typical 2138 cm^{-1} band, which can be assigned to CO interaction with the zeolitic framework. This assignment is further supported by the quick disappearance of the 2138 cm^{-1} band upon sample evacuation.

Figure 3 The Li^+-CO interaction at the T_3 position from two "opposite" side pockets: $T_3S(8R)/S$ ($-\Delta H_0$ = 44 kJ/mol and ν_{CO}=2182 cm^{-1}) (a) and $T_3S(8R)/S$ ($-\Delta H_0$ = 37 kJ/mol and ν_{CO}=2182 cm^{-1}) (b).

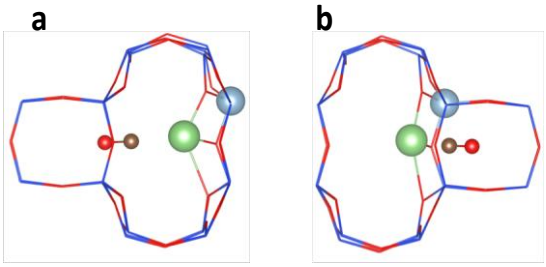

The Li^+-CO bands observed in our study are only partially consistent with previous studies. The *hf* band at 2188 cm^{-1} has been observed by Bordiga et al.,[10] but the *lf* band has not been observed. They did not rule out the possibility of Li^+ cation inside the side pockets; nevertheless, the main argument was that this CO band could be overshadowed by a strong BAS-CO adduct around 2170 cm^{-1}. Based on our measurements and calculations, it can be concluded that the Li^+ is present inside the constricted part of the **MOR** structure. On the other hand, it is most likely that the Li^+ exchange into this site cannot be done completely as suggested by Salla or Bordiga et al.,[10,16] where the 2161 cm^{-1} CO band remained after Li^+ exchange from the parent Na-MOR material. This finding is fully consistent with DFT calculations (the 2161 cm^{-1} band corresponds to the CO interaction with Na^+ located at the channel constriction, see Section 3.2).

The calorimetry measurement (Figure 4) has shown that Li^+-CO complexes have a similar isosteric heat due to the slow decrease from 45 kJ/mol to 34 kJ/mol. The most stable adsorption site yields isosteric heat of about 44 kJ/mol and corresponds to Al at the T_3 position, further supporting the presence of Li^+ at the channel constriction. The remaining isolated adsorption sites yield slightly lower isosteric heats (by 6–7 kJ/mol). The small differences between the adsorption sites inside the side pocket and the main channel can be

explained by Li^+ accessibility and CO dispersion interaction. The PBE interaction energies (Table 1) show that the lower dispersion contribution inside the main channel is compensated for by the stronger interaction of CO with the Li^+ cation.

Figure 4 The adsorption heats of CO interacting with LiH-**MOR**(9) (red circles), Na-**MOR**(9) (full blue squares), Na-**MOR**(40) (empty blue squares) and K-**MOR**(9) (green triangles) measured by adsorption microcalorimetry at 303 K. Inset: a detailed view of the zero-coverage limit of adsorption heat for Na-**MOR** zeolites.

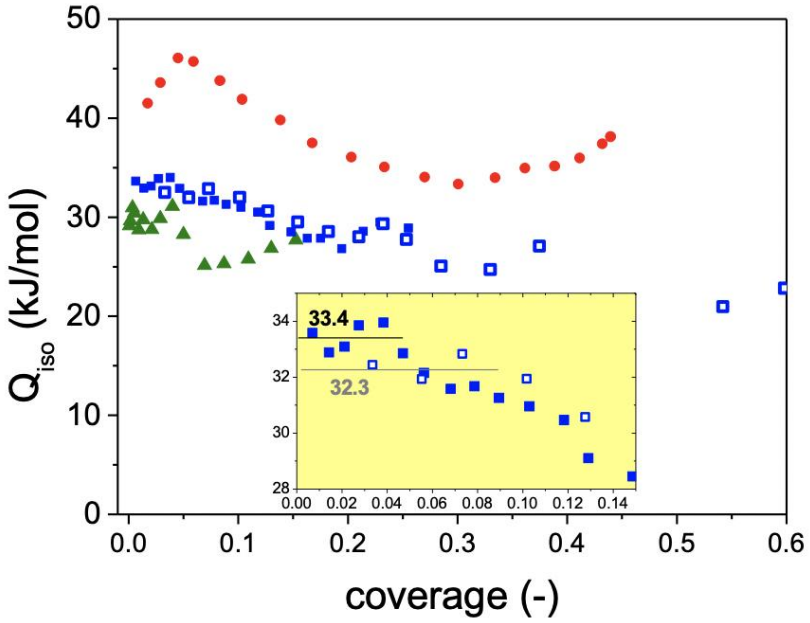

3.2 Na-MOR

The FT-IR spectra of CO adsorbed in Na-**MOR**(9,40) samples are shown in Figure 5 and theoretical calculations are summarized in Table 2. The FT-IR spectra of CO/Na-**MOR** exhibit three well-distinguished bands at 2177, 2165 and 2138 cm^{-1}. The behavior of the bands in the spectra of Na-**MOR**(9) (Figure 5A) and Na-**MOR**(40) (Figure 5B) is slightly different. In the case of Na-**MOR**(9), the bands have a constant position and the band at 2165 cm^{-1} has slower desorption dynamics than the band at 2179 cm^{-1}. On the contrary, with decreasing coverage, the maxima of the bands shift to higher wavenumbers (by several cm^{-1}) and the band at 2160–5 cm^{-1} is clearly less stable than the band at 2179 cm^{-1} in the case of Na-**MOR** (40). In addition, the population of both carbonyl types varies with the Si/Al ratio. The carbonyls characterized by the stretching frequency of 2160–5 cm^{-1} are more populated in **MOR**(40) than in the **MOR**(9) sample. Our measurements are in reasonable agreement with previous studies, but the intensities of *lf* and *hf* bands differ significantly even for samples with similar Si/Al ratios.[10,16] This indicates that the Al distribution in the framework is the key

factor to understand intensity changes in **MOR**(9,40) samples. Close inspection of the kinetics of CO adsorption for both samples (Figure S6) reveals a delayed appearance of the *lf* band in Na-**MOR**(9), indicating a slower diffusion into the side pockets. This type of behavior is not observed for a high-silica sample (i.e. Na-**MOR**(40)). For the further investigation of the CO interaction with sodium cations in **MOR** zeolites, the adsorption heats of CO were measured by microcalorimetry (Figure 4). The data obtained have shown that the differences in adsorption heats are insignificant, because both curves basically merge into one. Only the heats obtained by averaging the first few points (the heats for the zero-coverage limit) slightly differ – by ca 1 kJ/mol (see the inset in Figure 4).

Figure 5 The FT-IR spectra of the CO adsorbed at 77 K and subsequently gradually desorbed from the LASs of Na-**MOR**(9) (A), and Na-**MOR**(40) (B).

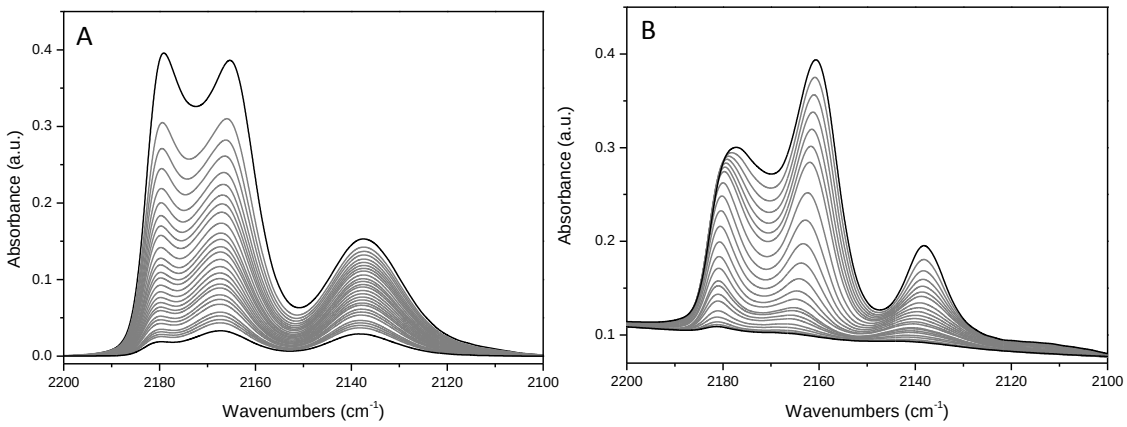

Table 2 The DFT/CC interaction energy and adsorption enthalpy (in kJ/mol) of CO on Na-**MOR** LASs along with *ω/r* CO frequencies (in cm^{-1}).

Ads. site[a]	E_{int}[b]	$-\Delta H_0$	ν_{CO}[c]	Band
T_1S(8R)/S	-37.3(-17.0)	34.4	2166	*lf*
T_1M(6R)/M	*-31.2(-24.4)*	*28.9*	*2177*	*hf*
T_2I(8R)/M	-33.4(-25.8)	30.9	2178	*hf*
T_2I(8R)/S[d]	-39.4(-20.0)	35.9	2181	*hf*
T_3S(8R)/S	-36.3(-14.3)	33.0	2162	*lf*
T_4I(8R)/M	-35.2(-26.8)	32.7	2180	*hf*
T_4I(8R)/S[d]	-37.9(-18.6)	34.6	2176	*hf*

[a] Less stable isolated sites are in italics (Table S4).

[b] PBE interaction energy is given in parentheses.

[c] CO gas-phase frequency is 2143 cm^{-1}.

[d] CO needs to pass through the channel constriction to form these adsorption complexes.

A comparison of the experimental results with theoretical calculations in Table 2 allows the assignment of the observed bands to individual carbonyl types and locations. The values in Table 2 were calculated for isolated Na^+ sites and as such are more consistent with the Na-**MOR**(40) sample. The *hf* band at 2177 cm^{-1} corresponds to CO interaction with Na-LASs at T_2 and T_4 intersection positions, the lower frequency around 2165 cm^{-1} clearly corresponds to cationic positions in the vicinity of the channel constriction (i.e. T_1 and T_3 positions) and the 2138 cm^{-1} band corresponds to the CO interaction with the channel wall. The observed desorption behavior of the Na-**MOR**(40) sample is also consistent with calculated PBE data. The lower stability of the *lf* band upon dynamic evacuation corresponds to a weaker CO interaction with Na-LASs at T_1 (T_1S vs. T_2I) and T_3 (T_3S vs. T_4I) positions. The small red shift in CO frequency with the increasing coverage of the Na-**MOR**(40) sample can be explained by the formation of dicarbonyl species on T_1 and T_3 adsorption sites (Figure S7). The shift is mainly manifested at the T_1 position, where the CO frequencies correspond to 2163–4 cm^{-1} and the adsorption enthalpy has decreased to 28.9 kJ/mol, whereas at the T_3 position the shift is only 1 cm^{-1} (i.e. 2161 cm^{-1}) and the adsorption decreases only to 31.8 kJ/mol, indicating that the interaction is of similar strength from both side pockets (Figure S7b).

3.3 K-MOR

The FT-IR spectra of CO adsorbed on K-**MOR**(9) are shown in Figure 6. The spectra are dominated by a main band at 2161 cm^{-1}, which shifts to 2165 cm^{-1} with decreasing coverage. The main band exhibits a not very clear shoulder at ca 2151 cm^{-1}. Furthermore, like in other samples, a band at 2138 cm^{-1} is visible in the spectra. In addition, there is a band at 2118 cm^{-1} in the spectra that coincides with the frequency of the isocarbonyls described in the potassium forms of MFI, FER and BEA zeolites.[26,31,46] The spectral features observed are very similar to those of Salla et al.,[16] but our interpretation based on theoretical results differs. The results of the theoretical calculation are summarized in Table 3. In the case of the K-**MOR(**9) sample, it is observable that CO shifts at different T positions start to coincide, although the best coordinated K^+ site at the T_3 position shows the lowest frequency. Moreover, the calculated isosteric heats start to be comparable to the CO interaction with channel walls inside the side pockets (E_{int}= -30 kJ/mol). As a result, the CO dynamics start to play an important role and the formation of O-end complexes (i.e. isocarbonyls) is expected and manifested in the FT-IR

spectra by the wide band around 2118 cm^{-1} (Figure 6). The increased stability of 2138 cm^{-1} is also observed (see Section 3.4). Actually, the K^+ positions in the **MOR** sample are the most distinctive because of the strong K^+ preference to exchange into 8-membered rings (Table S4 and Figure S5). CO desorption leads to the occurrence of the band around 2150 cm^{-1}, which can be assigned to dual cationic sites (see Section 3.5). At the moment, no clear explanation for the shift observed in CO upon desorption is available. However, it does not seem that dicarbonyl species are responsible for it, because their formation further weakens the interaction, as a result of which the observed red shift is significantly larger for one of the CO adsorbates (2144–6 cm^{-1}) and the second CO molecule is negligibly red-shifted with respect to the former K^+-CO adduct.

Figure 6 The FT-IR spectra of CO adsorbed at 77 K and subsequently gradually desorbed from the LASs of K-**MOR**(9)

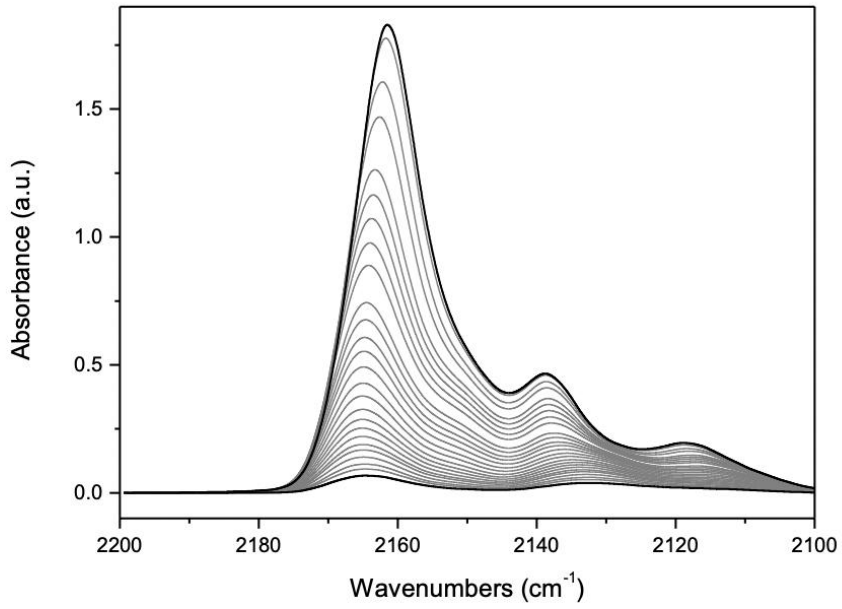

Table 3 The DFT/CC interaction energy and adsorption enthalpy (in kJ/mol) of CO on K-**MOR** LASs along with *ω/r* CO frequencies (in cm^{-1}).

Ads. site	E_{int} [a]	$-\Delta H_0$	ν_{CO} [b]
T_1S(8R)/S	-29.2(-9.7)	27.4	2164
T_2I(8R)/M	-24.1(-16.0)	22.2	2166
T_2I(8R)/S[c]	-30.3(-11.3)	27.8	2169
T_3S(8R)/S	-28.1(-8.6)	26.2	2162
T_4I(8R)/M	-23.4(-15.8)	21.8	2166
T_4I(8R)/S[c]	-30.6 (-11.8)	28.3	2166

[a] PBE interaction energy is given in parentheses.

[b] CO gas-phase frequency is 2143 cm^{-1}.

[c] CO needs to pass through the channel constriction to form these adsorption complexes.

3.4 The assignment of the band at 2138 cm^{-1} and the explanation of its behavior

The remaining question is why the band at 2138 cm^{-1} shows increased kinetic stability in Na/K-**MOR**(9) with respect to H/Li-**MOR**(9) and Na-**MOR**(40) samples. It is clear that the behavior of the band is influenced by the Si/Al ratio and exchange degree (Figure 7). The kinetics of desorption of the carbonyls assigned to the band at 2138 cm^{-1} are faster for **MOR** samples with small cations (proton and lithium), whereas sodium and potassium forms exhibit significantly higher kinetic stability. However, the kinetics of desorption are significantly accelerated if the Si/Al ratio is increased (cf. Na-**MOR**(9) and Na-**MOR**(40) in Fig. 7A) or if sodium occupies only a part of exchangeable sites (see Fig. 7B). The semi-logarithmic display of data (Fig S8) indicates that the kinetics of desorption on LiH- and Na(x)H-**MOR**(9) samples are more complex and consist of two processes (two linear regions are distinguishable in the curves). It is possible to rule out the formation of the dual cationic sites (DCSs) characterized by this band (see Section 3.5) as suggested by Salla et al.[16,21,47] The remaining explanation is that the increased kinetic stability is a result of the diffusion limitation of CO in **MOR** samples with larger cations causing steric hindrance. The main difference between protonic and lithium forms on the one hand and sodium and potassium forms on the other is that a sodium (or potassium) cation is large enough to block the intersection at T_2 and T_4 positions effectively and also prefers those positions, unlike Li^+. Furthermore, the Na/K-**MOR**(9) samples exhibit a "gate" effect in the measurement of nitrogen isotherm (Figure S4); therefore, there can a be delay upon diffusion from the material itself as a result of the larger concentration of the cations inside the main channel.

Figure 7 The time dependence of the intensity of the 2138 cm^{-1} band upon dynamic evacuation by a turbomolecular pump at 77K on various alkali metal **MOR** zeolites (A) and on partially ion-exchanged Na(x)H-**MOR**(9) samples.

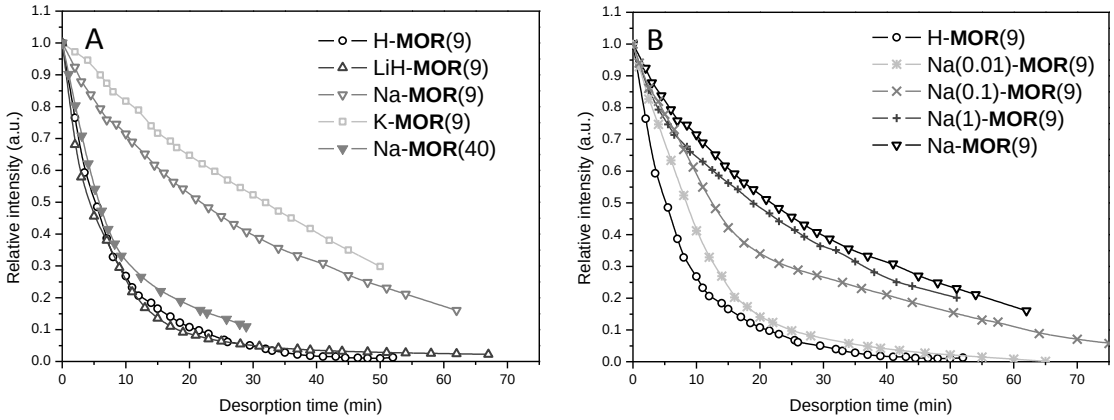

3.5 Dual cationic sites

The results for representative sets of Na-**MOR** DCSs are summarized in Table 4 (Figure 8). We have investigated ten different DCS arrangements with Na–Na distances ranging from 6.7 to 9.4 Å. It can be expected that DCSs are rather formed inside the main channel due to the fact that diffusion would exclude the formation of DCSs inside the side pockets. The calculated isosteric heats are between 28 and 32 kJ/mol, thus close to the results obtained for isolated sites (cf. Table 2). The median of the calculated CO shifts is 2165 cm^{-1}, with the lowest calculated shift being 2151 cm^{-1}, corresponding to the DCS with the shortest Na–Na distance of 6.7 Å. It is straightforward to conclude that the formation of DCSs on Na-**MOR** cannot be ruled out, but their formation will be most likely hidden in the 2165 cm^{-1} band (Figure 5).

We have investigated only a subset of intersection sites as a representative set for DCSs in K-**MOR.** The results are summarized in Table 5. The shoulder around 2150 cm^{-1} as observed in the FT-IR spectra of K-**MOR** (Figure 6) most likely corresponds to DCSs in the main channel. However, the isosteric heats of DCSs do not differ much from the isolated sites in the main channel, which makes it impossible to distinguish DCSs in calorimetric data.

Figure 8 The representative set of Na-**MOR** DCSs. The order a–e is based on Table 4.

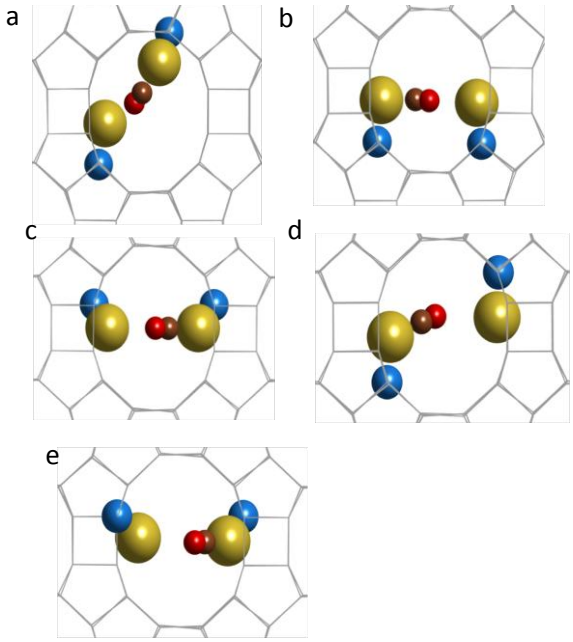

Table 4 The DFT/CC interaction energy and adsorption enthalpy (in kJ/mol) of CO on the DCSs of Na-**MOR** with *ω/r* CO frequencies (in cm^{-1}).

Ads. site[a]	r_{M-M}	E_{int}[b]	$-\Delta H_0$	ν_{CO}[c,d]
T_1M(6R)-T_2I(8R)/M	6.7	-33.9(-25.3)	31.4	2151
T_2I(8R)-T_2I(8R)/M	7.8	-31.6(-24.3)	29.0	2161
T_4I(8R)-T_4I(8R)/M	7.9	-31.6(-25.8)	29.2	2167
T_2I(8R)-T_2I(8R)/M	8.6	-33.3(-25.6)	30.9	2168
T_4I(8R)-T_4I(8R)/M	9.4	-34.6(-26.4)	32.1	2169

[a] The adsorption sites are shown in Figure 8a–e according to their order in this table.

[b] PBE interaction energy is given in parentheses.

[c] CO gas-phase frequency is 2143 cm^{-1}.

[d] The *ω/r* CO frequencies have been calculated from the average of C- and O-end correlations (Table S2).

Table 5 The DFT/CC interaction energy and adsorption enthalpy (in kJ/mol) of CO on the DCSs of K-**MOR** with *ω/r* CO frequencies (in cm^{-1}).

Ads. site[a]	r_{M-M}	E_{int}[b]	$-\Delta H_0$	ν_{CO}[c,d]
T_2I(8R)-T_2I(8R)/M	7.8	-24.4(-18.0)	22.6	2147
T_4I(8R)-T_4I(8R)/M	8.0	-23.0(-17.5)	21.2	2150
T_2I(8R)-T_2I(8R)/M	8.2	-22.4(-16.4)	20.6	2152
T_4I(8R)-T_4I(8R)/M	8.7	-23.2(-16.3)	21.3	2152

[a] The adsorption sites are analogical to those defined in Figure 8c–e.

[b] PBE interaction energy is given in parentheses.

[c] CO gas-phase frequency is 2143 cm^{-1}.

[d] The *ω/r* CO frequencies have been calculated from the average of C- and O-end correlations (Table S2).

Conclusions

The careful experimental and theoretical re-examination of CO interaction with alkali metal-exchanged **MOR** materials has led to the following conclusions. The Li^+ at least partially exchanges into the constricted part of the **MOR** material as evidenced by the low-frequency band and the corresponding larger isosteric heats observed inside LiH-**MOR** side pockets. In the case of sodium exchange, we have measured two **MOR** samples with the Si/Al ratio of 40 and 9, respectively. Our measurements and calculations support previous assignments of low- and high-frequency bands, corresponding to the sodium sites inside the side-pockets and the main channel. However, the kinetic stability of low- and high-frequency bands differs upon evacuation, which can most likely be explained by diffusion limitations. This assumption has been confirmed by additional kinetic measurements, which have clearly shown a delayed appearance of a low-frequency band in Na-**MOR**(9). Moreover, the IR intensities of carbonyl species significantly differ between the two investigated Na-**MOR** samples, indicating a key factor of Al distribution in **MOR** materials. Considering the formation of dual cationic sites in Na-**MOR**(9), it can be concluded that their IR band would be quite close to the IR bands of isolated sites and with no significant enthalpy gain to distinguish them in calorimetry measurements. In the case of K-**MOR**, we have observed a significant decrease in the differences between the sites in the main channel and side pockets, unlike in the case of Li^+ and Na^+. This is mainly caused by the fact that the interaction of CO with the potassium cation is the weakest and the interaction with the framework starts to compete with the formation of a K^+-CO adduct. As a result, it is also possible to observe the isocarbonyl species in the IR spectra. Furthermore, the formation of dual cationic sites is manifested in the spectra by the weak band around 2150 cm^{-1} as confirmed by model calculations. The remaining puzzling question is the increased kinetic stability of the 2138 cm^{-1} band in Na/K-**MOR**(9) with respect to H/Li-**MOR** or Na-**MOR**(40). Based on our measurements, there seems to be a steric hindrance caused by larger cations. This conclusion is further supported by the observed "gate" effects in the measurement of N_2 adsorption isotherms.

Acknowledgement

The authors acknowledge the financial support of the Czech Science Foundation under project No. 17-07642S. Computational resources were provided by the Ministry of Education, Youth and Sports of the Czech Republic from the Large Infrastructures for Research, Experimental Development and Innovations project (IT4Innovations National Supercomputing Center) and by the CESNET and the CERIT Scientific Cloud (Grants No. LM2015070, LM2015042, and LM2015085).

Supporting Information

The SI contains the basic material characterization in Table S1 and Figures S1 and S2 and theoretical foundations such as ω/r parameters (Table S2) and CCSD(T)/CBS benchmarks (Table S3). The cation-site stabilities are provided in Table S4 and depicted in Figures S3–S5. The kinetic measurements are shown in Figure S6 and possible structures of dicarbonyl species are illustrated in Figure S7. The stability of the 2138 cm^{-1} band upon dynamic evacuation is depicted in Figure S8.

References

(1) *Zeolite microporous solids: Synthesis, structure and reactivity*; Derouane, E. G.; Lemos, F.; Naccache, C., Eds.; 1st ed.; Springer Science+Business Media Dordrecht, 1992.
(2) Li, Y.; Li, L.; Yu, J. *Chem* **2017**, *3*, 928–949.
(3) Chibani, S.; Chebbi, M.; Lebègue, S.; Bučko, T.; Badawi, M. *J. Chem. Phys.* **2016**, *144*.
(4) Cherkasov, N.; Vazhnova, T.; Lukyanov, D. B. *Vib. Spectrosc.* **2016**, *83*, 170–179.
(5) Webster, C. E.; Cottone, A.; Drago, R. S. *J. Am. Chem. Soc.* **1999**, *121*, 12127–12139.
(6) Alberti, A. *Zeolites* **1997**, *19*, 411–415.
(7) Makarova, M. A.; Wilson, A. E.; Van Liemt, B. J.; Mesters, C. M. A. M.; De Winter, A. W.; Williams, C. *J. Catal.* **1997**, *172*, 170–177.
(8) Lee, C.; Parrillo, D. J.; Gorte, R. J.; Farneth, W. E. *J. Am. Chem. Soc.* **1996**, *118*, 3262–3268.
(9) Maache, M.; Janin, A.; Lavalley, J. C.; Benazzi, E. *Zeolites* **1995**, *15*, 507–516.
(10) Bordiga, S.; Lamberti, C.; Geobaldo, F.; Zecchina, A.; Palomino, G. T.; Areán, C. O. *Langmuir* **1995**, *11*, 527–533.
(11) Geobaldo, F.; Lamberti, C.; Ricchiardi, G.; Bordiga, S.; Zecchina, A.; Palomino, G. T.; Areán, C. O. *J. Phys. Chem.* **1995**, *99*, 11167–11177.
(12) Zholobenko, V. L.; Makarova, M. A.; Dwyer, J. *J. Phys. Chem.* **1993**, *97*, 5962–5964.
(13) Wakabayashi, F.; Kondo, J.; Wada, A.; Domen, K.; Hirose, C. *J. Phys. Chem.* **1993**, *97*, 10761–10768.
(14) Lamberti, C.; Bordiga, S.; Geobaldo, F.; Zecchina, A.; Otero Areán, C. *J. Chem. Phys.* **1995**, *103*, 3158–3165.

(15) Díaz Soto, L.; Sierraalta, A.; Añez, R.; Nascimento, M. A. C. *J. Phys. Chem. C* **2015**, *119*, 8112–8123.
(16) Salla, I.; Montanari, T.; Salagre, P.; Cesteros, Y. ; Busca, G.; *Phys. Chem. Chem. Phys.* **2005**, *7*, 2526–2533.
(17) de S. Vilhena, F.; Serra, R. M.; Boix, A. V.; Ferreira, G. B.; José, J. W. *Comput. Theor. Chem.* **2016**, *1091*, 115–121.
(18) Villarreal, A.; Garbarino, G.; Riani, P.; Finocchio, E.; Bosio, B.; Ramírez, J.; Busca, G. *J. CO2 Util.* **2017**, *19*, 266–275.
(19) Lukyanov, D. B.; Vazhnova, T.; Cherkasov, N.; Casci, J. L.; Birtill, J. J. *J. Phys. Chem. C* **2014**, *118*, 23918–23929.
(20) Delgado, J. A.; Uguina, M. A.; Gómez, J. M.; Ortega, L. *Sep. Purif. Technol.* **2006**, *48*, 223–228.
(21) Salla, I.; Montanari, T.; Salagre, P.; Cesteros, Y.; Busca, G. *J. Phys. Chem. B* **2005**, *109*, 915–922.
(22) Marie, O.; Massiani, P.; Thibault-Starzyk, F. *J. Phys. Chem. B* **2004**, *108*, 5073–5081.
(23) Nesterenko, N. S.; Thibault-Starzyk, F.; Montouillout, V.; Yuschenko, V. V; Fernandez, C.; Gilson, J. P.; Fajula, F.; Ivanova, I. I. *Microporous Mesoporous Mater.* **2004**, *71*, 157–166.
(24) Demuth, T.; Hafner, J.; Benco, L.; Toulhoat, H. *J. Phys. Chem. B* **2000**, *104*, 4593–4607.
(25) Veefkind, V. A.; Smidt, M. L.; Lercher, J. A. *Appl. Catal. A Gen.* **2000**, *194*, 319–332.
(26) Garrone, E.; Bulánek, R.; Frolich, K.; Areán, C. O.; Delgado, M. R.; Palomino, G. T.; Nachtigallová, D.; Nachtigall, P. *J. Phys. Chem. B* **2006**, *110*, 22542–22550.
(27) Rubeš, M.; Koudelková, E.; De Oliveira Ramos, F. S.; Trachta, M.; Bludský, O.; Bulánek, R. *J. Phys. Chem. C* **2018**, *122*, 6128-6136.
(28) Rubeš, M.; Trachta, M.; Koudelková, E.; Bulánek, R.; Klimeš, J.; Nachtigall, P.; Bludský, O. *J. Phys. Chem. C* **2018**, *122*, 26088–26095.
(29) Nachtigall, P.; Bulanek, R. *Appl. Catal. A* **2006**, *307*, 118–127.
(30) Nachtigall, P.; Bludský, O.; Grajciar, L.; Nachtigallová, D.; Delgado, M. R.; Areán, C. O. *Phys. Chem. Chem. Phys.* **2009**, *11*, 791–802.
(31) Nachtigall, P.; Rodríguez Delgado, M.; Frolich, K.; Bulánek, R.; Turnes Palomino, G.; López Bauçà, C.; Otero Areán, C. *Microporous Mesoporous Mater.* **2007**, *106*, 162–173.
(32) Bordiga, S.; Lamberti, C.; Bonino, F.; Travert, A.; Thibault-Starzyk, F. *Chem. Soc. Rev.* **2015**, *44*, 7262–7341.
(33) Díaz Soto, L. J.; Sierraalta, A.; Añez, R.; Nascimento, M. A. C. *Appl. Catal. A Gen.* **2016**, *526*, 53–61.
(34) Bulánek, R.; Koudelková, E.; Solanea de Oliveira Ramos, F.; Trachta, M.; Bludský, O.; Rubeš, M.; Čejka, J. *Microporous Mesoporous Mater.* **2019**, *280*, 203–210.
(35) Bludský, O.; Rubeš, M.; Soldán, P.; Nachtigall, P. *J. Chem. Phys.* **2008**, *128*, 1–8.
(36) Alberti, A.; Davoli, P.; Vezzalini, G. *Zeitschrift fur Krist. – New Cryst. Struct.* **1986**, *175*, 249–256.
(37) Brändle, M.; Sauer, J. *J. Am. Chem. Soc.* **1998**, *120*, 1556–1570.
(38) Sasaki, H.; Oumi, Y.; Itabashi, K.; Lu, B.; Teranishi, T.; Sano, T. *J. Mater. Chem.* **2003**, *13*, 1173–1179.
(39) Perdew, J.; Burke, K.; Ernzerhof, M. *Phys. Rev. Lett.* **1996**, *77*, 3865–3868.
(40) Baerlocher, C.; McCusker, L. B. Database of Zeolite Structures.
(41) Blochl, P. *Phys. Rev. B* **1994**, *50*, 17953.
(42) Kresse, G.; Hafner, J. *Phys. Rev. B* **1993**, *48*, 13115.
(43) Nachtigallová, D.; Nachtigall, P.; Bludský, O. *Phys. Chem. Chem. Phys.* **2004**, *6*,

5580–5587.
(44) Bartlett, R.; Musial, M. *Rev. Mod. Phys.* **2007**, *79*, 291.
(45) Henkelman, G.; Jónsson, H. *J. Chem. Phys.* **1999**, *111*, 7010–7022.
(46) Bulánek, R.; Koudelková, E. *Microporous Mesoporous Mater.* **2012**, *151*, 149–156.
(47) Montanari, T.; Kozyra, P.; Salla, I.; Datka, J.; Salagre, P.; Busca, G. *J. Mater. Chem.* **2006**, *16*, 995–1000.

Supplementary Material

Click here to download Supplementary Material: SI_verze_final.docx

***Declaration of Interest Statement**

Declaration of interests

☒ The authors declare that they have no known competing financial interests or personal relationships that could have appeared to influence the work reported in this paper.

☐The authors declare the following financial interests/personal relationships which may be considered as potential competing interests: